IOP Publishing Journal of Neural Engineering
J. Neural Eng. 13 (2016) 046016 (12pp) doi:10.1088/1741-2560/13/4/046016

SiC protective coating for photovoltaic retinal prosthesis

Xin Lei[1], Sheryl Kane[2,7], Stuart Cogan[3], Henri Lorach[4,5], Ludwig Galambos[1], Philip Huie[4,5], Keith Mathieson[6], Theodore Kamins[1], James Harris[1] and Daniel Palanker[4,5]

[1] Department of Electrical Engineering, Stanford University, Stanford, CA, USA
[2] Work performed at EIC Laboratories, Norwood, MA, USA
[3] University of Texas at Dallas, Richardson, TX, USA
[4] Hansen Experimental Physics Laboratory, Stanford University, Stanford, CA, USA
[5] Department of Ophthalmology, Stanford University, Stanford, CA, USA
[6] Institute of Photonics, Department of Physics, SUPA, University of Strathclyde, Glasgow, Scotland, UK

E-mail: leixin@stanford.edu

Received 12 September 2015, revised 10 February 2016
Accepted for publication 23 May 2016
Published 21 June 2016

Abstract

Objective. To evaluate plasma-enhanced, chemically vapor deposited (PECVD) amorphous silicon carbide (α-SiC:H) as a protective coating for retinal prostheses and other implantable devices, and to study their failure mechanisms *in vivo*. *Approach.* Retinal prostheses were implanted in rats sub-retinally for up to 1 year. Degradation of implants was characterized by optical and scanning electron microscopy. Dissolution rates of SiC, SiN_x and thermal SiO_2 were measured in accelerated soaking tests in saline at 87 °C. Defects in SiC films were revealed and analyzed by selectively removing the materials underneath those defects. *Main results.* At 87 °C SiN_x dissolved at 18.3 $\pm$ 0.3 nm d^{-1}, while SiO_2 grown at high temperature (1000 °C) dissolved at 0.104 $\pm$ 0.008 nm d^{-1}. SiC films demonstrated the best stability, with no quantifiable change after 112 d. Defects in thin SiC films appeared primarily over complicated topography and rough surfaces. *Significance.* SiC coatings demonstrating no erosion in accelerated aging test for 112 d at 87 °C, equivalent to about 10 years *in vivo*, can offer effective protection of the implants. Photovoltaic retinal prostheses with PECVD SiC coatings exhibited effective protection from erosion during the 4 month follow-up *in vivo*. The optimal thickness of SiC layers is about 560 nm, as defined by anti-reflective properties and by sufficient coverage to eliminate defects.

Keywords: SiC, silicon carbide, retinal prostheses, protective coating, neural stimulation, chronic implant

(Some figures may appear in colour only in the online journal)

Introduction

The spectrum of implantable electro-neural interfaces for restoration and control of sensory, motor, and other brain functions is rapidly expanding. Examples include cochlear implants [1–3], deep brain stimulators [4–7], cortical motor prostheses [8–10], cortical visual prostheses [11, 12] and retinal prostheses [13–17], amongst others. The majority of electrical implants employ metal or ceramic enclosures with cable feed-throughs to protect the electronics from exposure to body fluids and associated corrosion [10, 14, 15, 18]. This approach results in rather bulky implants and difficult surgeries that involve separate placements for the power supplies and electrode arrays, and routing of interconnecting cables.

Our group developed a silicon photodiode array implanted sub-retinally for restoration of sight to patients blinded by degenerative retinal diseases, such as age-related macular degeneration and retinitis pigmentosa [16, 17]. With pulsed near-infrared light providing both power and visual

[7] Present address: Amgen, Cambridge, Massachusetts, USA.

information, the implant is completely wireless, greatly reducing implant size and simplifying surgery.

Since this implant is not packaged in a hermetic metal enclosure, it is exposed to body fluids. Without an optimized protective coating, the device remained functional in short-term (under 1 year) studies *in vitro* and *in vivo*, but with detectable degradation. For long-term use of integrated circuit (IC) and micro-electro-mechanical systems (MEMS)-based biomedical devices, a biocompatible encapsulation layer is necessary to provide stable protection against water and ion ingress.

Dielectric materials deposited by low-pressure chemical vapor deposition (LPCVD) at high temperatures (800 °C–900 °C) have exhibited good stability and barrier properties in long-term *in vivo* studies [19–21]. However, such temperatures are incompatible with encapsulation of ICs. Development of an encapsulation layer which can be deposited at temperatures below 400 °C would be tremendously beneficial since it would allow its use for protection of ICs [22]. Low temperature (395 °C) LPCVD silicon oxide (SiO_2) implanted sub-retinally in rabbits was found to dissolve after 6–12 months [23]. Polymers, such as Parylene, are used in the medical industry for encapsulation of the neural implants [24–26]. Due to its low relative permittivity, high resistivity, biocompatibility and conformal deposition, Parylene is suitable as an electrical isolation material for implantable devices. Adhesion of Parylene to inorganic substrates can be improved by adhesion promoter and thermal treatment [27]. However, Parylene has relatively high water vapor transmission rate compared to many dielectric materials [26, 28], therefore Parylene by itself is not sufficient to protect implanted ICs. Atomic layer deposited Al_2O_3 is conformal and hermetic, yet found to dissolve in water [26, 29]. An Al_2O_3 and Parylene bilayer structure was proposed to improve its resistance to moisture and the encapsulation lifetime [26]. Diamond-like carbon coatings [30] and ultra-nano-crystalline diamond coatings [31–33] have demonstrated biocompatibility, resistance to corrosion and wear, and are being used in medical implants, with some concerns regarding delamination in an aqueous environment caused by high residual stress, leakage current, pinholes near sharp corners, and a relatively high deposition temperature.

As an alternative, amorphous silicon carbide (α-SiC:H) deposited at a low temperature was proposed as a protective coating due to its availability in semiconductor processing, compatibility with IC technology, biocompatibility [34–36], contamination barrier properties [37–40] and low dissolution rate in saline, compared to other commonly used dielectric materials for IC passivation, such as silicon nitride (SiN_x) and low-temperature SiO_2 [41–44].

In this study, we implanted retinal prosthetic devices for up to 1 year and characterized their degradation by optical and scanning electron microscopy (SEM) to assess the device failure mechanisms *in vivo*. We also measured the dissolution rates of SiC, SiN_x and thermal SiO_2 in accelerated soaking tests to compare stability of those dielectric materials. We revealed and analyzed the defects in SiC films, and defined the optimal thickness of SiC layer for reliable protection of the chronic implants.

Methods

Material deposition

Amorphous silicon carbide (α-SiC:H) was deposited by plasma-enhanced chemical vapor deposition (PECVD) at EIC Laboratories, Inc. (Norwood, MA). The precursors were SiH_4 and CH_4 (1:3 ratio of SiH_4/CH_4) in an Ar carrier gas. The deposition temperature was 325 °C at a pressure of 800 mTorr and an RF power frequency of 13.56 MHz. The SiN_x used in dissolution rate tests was deposited by PECVD at the Stanford Nanofabrication Facility (SNF) using surface technology systems (STS) PECVD. The precursors were SiH_4 and NH_3 (40:33.5 ratio of SiH_4/NH_3) at a deposition temperature of 350 °C and pressure of 650 mTorr. Dual frequency (13.56 MHz and 187.5 kHz) deposition was used. SiN_x was deposited as the top surface coating of retinal prostheses by PECVD at SNF (Plasma-Therm Shuttlelock SLR-730-PECVD). This tool used a capacitive-coupled plasma with 13.56 MHz RF power. Precursors were SiH_4 and NH_3 (5:3 ratio of SiH_4/NH_3), with He and N_2 carrier gases. The deposition temperature was 350 °C at a pressure of 950 mTorr. SiO_2 was grown by wet thermal oxidation in a resistance-heated oxidation furnace at 1000 °C.

Device fabrication

Three types of structures were used in this study. To minimize confusion, they are denoted as Type I, II and III, respectively.

Type I structures are retinal prosthetic implants fabricated at SNF using complementary metal–oxide–semiconductor and MEMS technologies. The fabrication process includes eight lithography steps on silicon-on-insulator wafers with 30 μm silicon device layers [45]. Each implant consists of an array of 142 hexagonal pixels, which are 70 μm in width. An individual pixel contains 2 or 3 photodiodes connected in series between active and return electrodes. Photodiodes and pixels are isolated by 5 μm wide trenches filled with undoped polysilicon (figure 1(a)). The implants are 1 mm in diameter and 30 μm thick. The main difference in the current devices from the previously described devices [45] is that the electrodes are connected to PN junctions with the opposite polarity—the active electrode connected to the p-type silicon region. This provides anodic-first pulses of current, optimal for sub-retinal stimulation [18, 46]. Devices were fabricated on two wafers, both having 60 nm of PECVD SiN_x (Plasma-Therm) on top of 70–80 nm of thermally grown SiO_2 (thermal oxide) on the surface. One wafer has an additional 240 nm layer of SiC on the top surface. The backside and sidewalls of all implants were covered with 480 nm of thermally grown SiO_2. Three Type I implants from each wafer were used in *in vivo* experiments. All of the 142 pixels of each implant were tested.

To facilitate defect analysis in SiC coatings, Type II structures were fabricated similarly to Type I devices but on

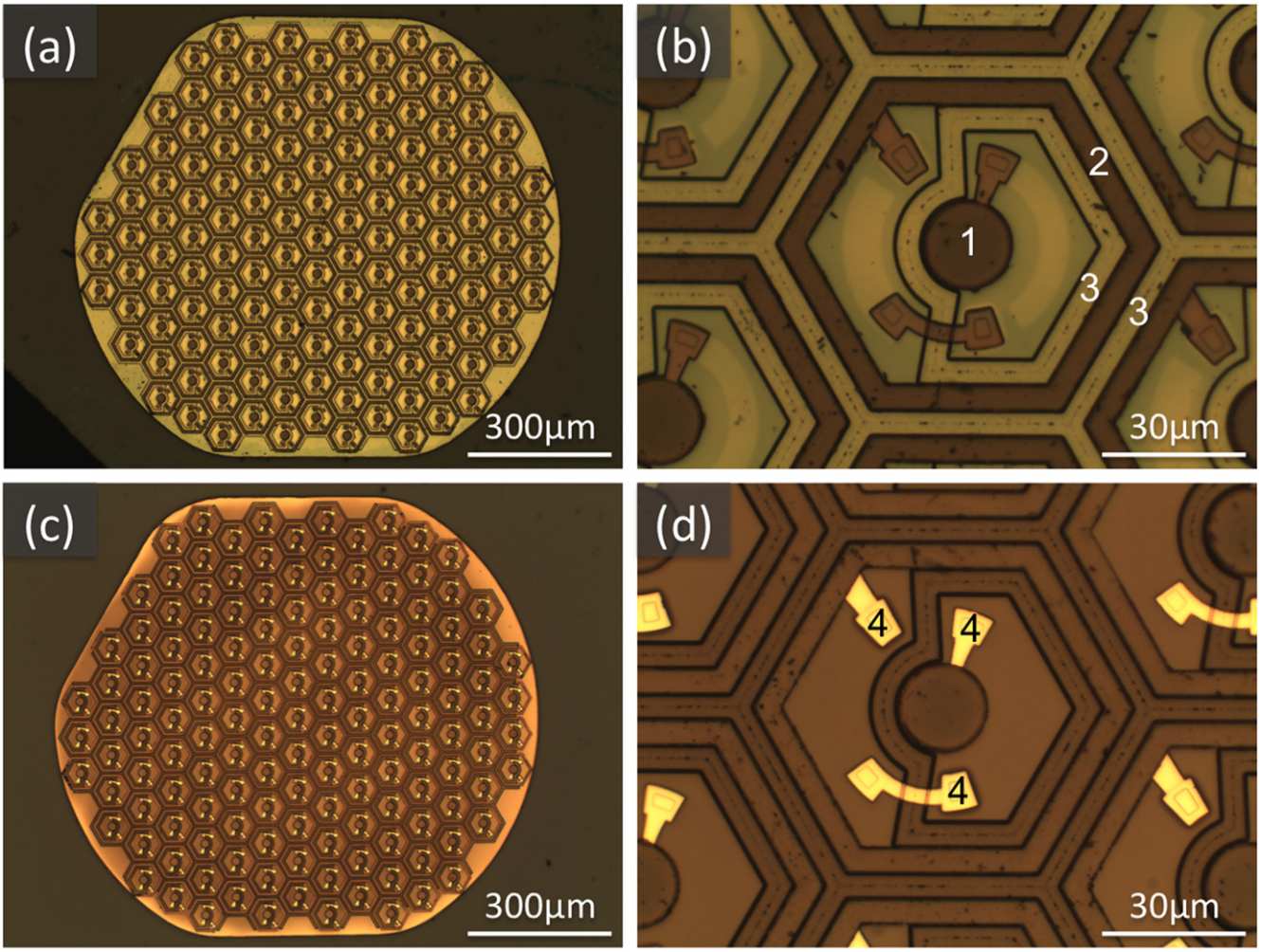

Figure 1. Optical microscopy of retinal prostheses (Type I) without SiC coating. (a) A 2-diode pixel device before implantation. (b) One pixel of the device in (a); 1—active electrode, 2—return electrode, 3—trenches filled with polysilicon. (c) and (d) Four months after sub-retinal implantation in a rat eye. The drastic color change and exposed metal wires (4, bright yellow) indicate the dissolution of SiN_x.

bulk silicon wafers, making the total array thickness ~520 μm. In addition to the 240 nm thick SiC films, some of Type II arrays had a thicker SiC coating—560 nm. These thick arrays were not used for *in vivo* experiments.

Type III structures are bulk silicon substrates (520 μm thickness) with 5 μm wide and 33 μm deep trenches etched using the Bosch process (Surface Technology Systems STSetch2) at SNF. A thermal oxidation at 1000 °C for 100 min followed the trench etching to conformally grow 480 nm SiO_2 on the samples. SiC films of 560 nm thickness were then deposited on the top surface of some samples, and 180 nm thick SiC films were deposited on others. Type III structures were used for the defect analysis, but not for *in vivo* experiments.

In vivo experiments

Each of the six Type I retinal prostheses (three with SiC coating and three without) were implanted sub-retinally in a different rat (six rats in total). The implantation technique was similar to the one previously reported by our group [17, 47] and performed in agreement with Stanford University institutional guidelines and the Statement for the Use of Animals in Ophthalmic and Vision Research. After a period of time (from 4 months to 1 year), implants were extracted from the tissue and cleaned in an enzyme solution (Tergazyme, 1%) for 1 d, and then further cleaned with deionized water and isopropyl alcohol (IPA). Explanted devices were examined with optical microscopy and SEM. Some devices were sputter coated with a thin layer of metal (~10 nm) to improve the SEM imaging by reducing the charging effects. It was not always possible to compare the same device and the same pixel before and after the implantation due to randomness of the defect locations. However, each optical and SEM image is representative of the type of implant in terms of the device structure and changes after the implantation.

Dissolution rate

Dissolution rates of dielectric materials in saline were measured in accelerated soaking tests. SiC, SiN_x, and SiO_2-coated

silicon substrates (520 μm thickness) were sealed in glass vials filled with saline, and placed in an oven with the temperature maintained at 87 °C for up to 112 d. Samples were periodically taken out of the chamber, rinsed with deionized water, dried and analyzed. The dissolution rate study at elevated temperature was performed in a low-phosphate saline (LPS), comprised of 126 mM NaCl, 5 mM Na_2HPO_4, and 1.4 mM NaH_2PO_4.

Five samples each of the SiC, SiN_x and SiO_2 coatings were used in the accelerated aging tests. SiC and SiN_x were grown on double-side polished silicon substrates. Before the soaking test, the thickness of SiC and SiN_x films was directly measured by selectively etching away the dielectric materials in a small region and measuring the step using surface profilometry. SiC films were 694 ± 10 nm thick on each side, and SiN_x films were 520 ± 5 nm thick on each side. SiO_2 films were grown on single-side polished silicon substrates. Thickness of SiO_2 films on silicon substrates was measured using spectral reflectometry (Nanometrics Nanospec 210XP), assuming the refractive index of SiO_2 to be 1.45 in the visible range. The five SiO_2 samples were found to be 511 ± 3 nm thick.

During the soaking tests of SiC and SiN_x, transmission-mode Fourier transform infrared spectroscopy (FTIR, Nicolet 6700) measurements were taken periodically on each sample to monitor changes of the films. The transmission FTIR spectra peaks were fitted, assuming Gaussian peak shapes, near the Si–C (~758 cm^{-1}) or Si–N (~820 cm^{-1}, 930 cm^{-1}) stretch frequencies, and the areas under the peaks were integrated. Prior to the soaking tests, we calibrated the integrated areas of fitted Gaussian peaks measured by FTIR to the thickness measured by surface profilometry by linear regression on samples of four different thicknesses for both SiC and SiN_x. All subsequent FTIR peak areas were converted to film thickness using these fitted linear models. Assuming the dissolution rates on both sides of the sample exposed to the same electrolyte are the same, the dissolution rate of a single exposed surface was calculated as half of the observed dissolution rate from two surfaces. For SiO_2 films, spectral reflectometry was performed periodically during the soaking test. The dissolution rate of each film was calculated by plotting the total film thickness versus soaking time.

Defect analysis

Defect analysis was performed only on SiC films since all other coatings were gradually dissolving. To reveal the defects in the SiC films, Type II arrays were soaked in buffered oxide etch (BOE) 6:1 (volume ratio of 40% NH_4F in water to 49% HF in water) for 10 min to etch SiN_x and SiO_2 through any defects in the SiC films. After etching, the defects became visible under an optical microscope. Type III structures were analyzed similarly by etching materials underneath the SiC to reveal defects in the SiC films. Specifically, samples were soaked in BOE 6:1 for 7 min to etch SiO_2. Some samples were further etched isotropically by xenon difluoride (XeF_2) gas (Xactix e-1) to remove several microns of silicon. For cross-sectional SEM analysis of samples coated with 560 nm SiC films, an additional SiO_2 etch in BOE 6:1 for 40 s was performed after cross sectioning the sample in order to recess the oxide and emphasize the SiC layer.

Results

Degradation of the implants in vivo

Implants without SiC coating degraded significantly during the 4 month sub-retinal implantation. SiN_x layer was completely dissolved on all pixels and devices, which was evident from the color change of the devices after implantation (figures 1(c) and (d) compared to 1(a) and (b)). Platinum wires connecting the PN junctions to electrodes became exposed (figure 1(d)). On one implant, polysilicon in the trench started to degrade (figure 2(c)), while on the other implant (figure 2(b)), this region did not show any visible changes (figure 2(a)).

All pixels without SiC coating implanted for 1 year showed visible degradation. However, the degradation was not uniform across a device, as shown in figure 3(a); some pixels exhibit more degradation than others. In some of the trenches, polysilicon was completely dissolved, leaving a thin SiO_2 membrane covering the trench top (figure 3(b), 1). As a result, the metal wires on top of these empty trenches were mechanically compromised (figures 3(b), 2, and (c), 2). Some thin SiO_2 films that originally covered the trench top were displaced after the polysilicon underneath was dissolved (figures 3(c), 3).

Despite the degradation, the implanted devices continued to function until they were explanted at least 7 months later [17], indicating that the SiO_2 films with metal wires on top of the empty trenches were displaced only during explantation (figure 3). Prolonged exposure of the implants *in vivo* will eventually lead to complete dissolution of the polysilicon in the trenches, which is likely to result in the loss of mechanical support, leading to device failure. During very long *in vivo* exposure, we speculate that the 70 nm of SiO_2 will eventually dissolve as well [48]. Once the active area (single-crystal silicon) of the devices is exposed to physiological environment, the silicon is expected to dissolve rapidly [43], and the devices will eventually stop functioning.

To evaluate the protective properties of SiC, three devices with 240 nm of SiC coating were implanted in three different rats for 4 months. One implant did not show any visible degradation under the optical microscope (figures 4(c) and (d)). Two other implants had minor degradation at isolated defect points, visible as small patches of color change near the middle of the polysilicon-filled trenches (figures 4(e) and (f), arrows) compared to the image before implantation (figures 4(a) and (b)). These defects were seen on 51 out of 142 pixels on one device, and 41 out of 142 on another. The patches of color changes indicate the presence of defects in the SiC films near the middle of the polysilicon-filled trenches, which allowed dissolution of the underlying SiN_x.

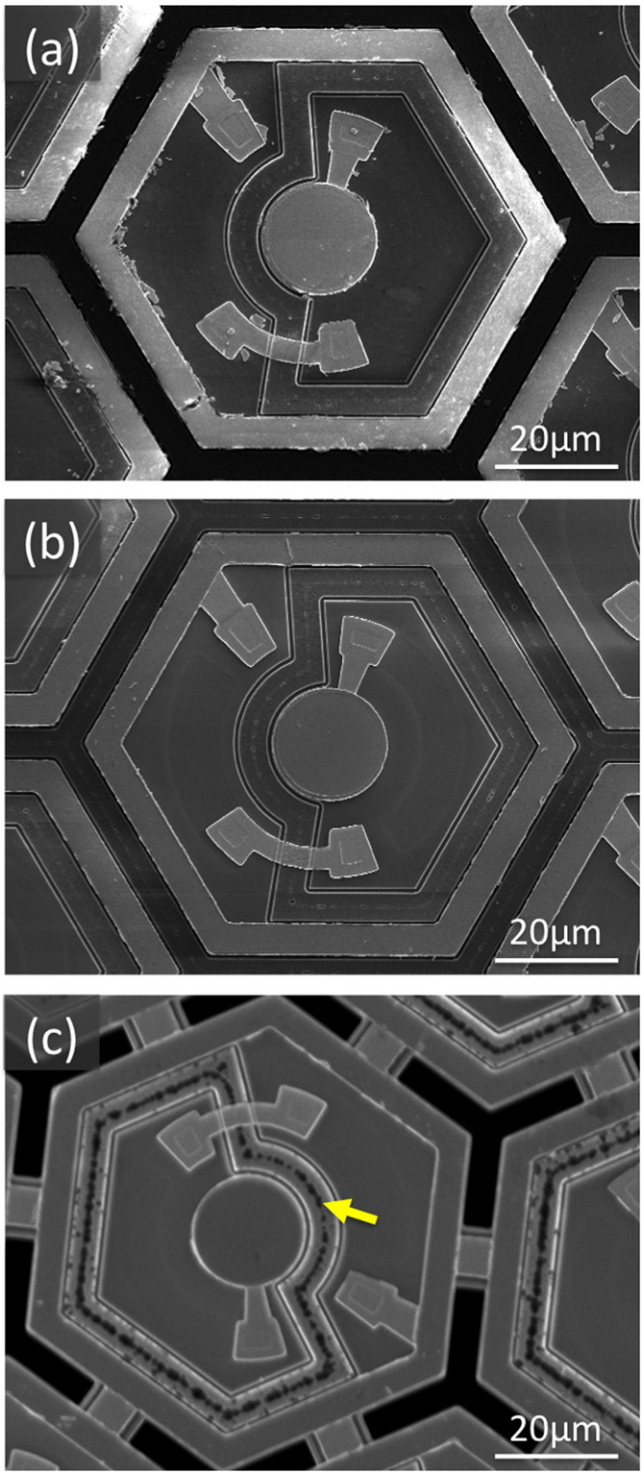

Figure 2. Scanning electron microscopy of retinal prostheses (Type I) without SiC coating. (a) A 2-diode pixel before implantation. (b) and (c) Four months after sub-retinal implantation in a rat eye. The implant in (c) exhibits degradation in the polysilicon trench region (arrow), while (b) did not show visible changes compared to (a). All implants shown in this figure are from the same wafer. Only one pixel of each implant is shown, but all pixels on an implant have similar degradation.

In summary, unprotected retinal implants degrade during prolonged *in vivo* exposure, while SiC films provided effective protection of the implants.

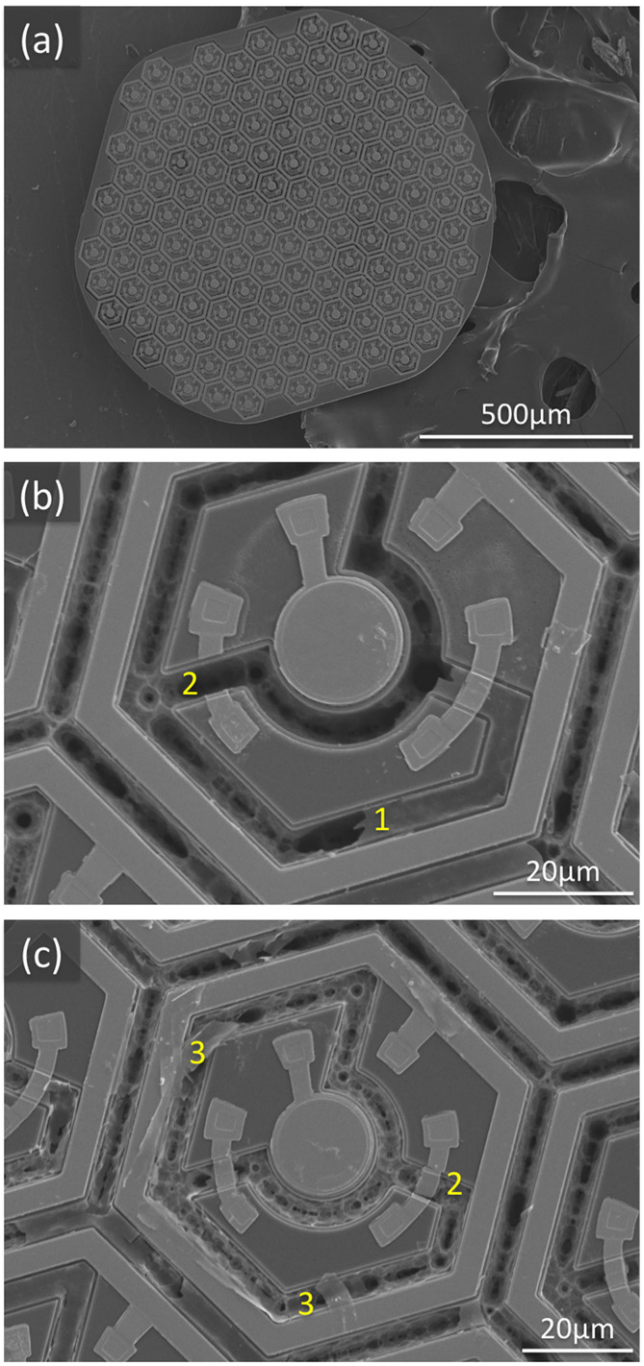

Figure 3. Scanning electron microscopy of retinal prostheses (Type I) without SiC coating after 1-year implantation. (a) All pixels in this device have visible degradation, albeit not uniform across the device. Both 3-diode pixels in (b) and (c) exhibit significant degradation. Polysilicon in some trenches is largely dissolved, leaving only a thin SiO_2 film covering the trench top (b1). Metal wires on top of the dissolved trenches could break (b2), (c2). Some SiO_2 films that originally covered the trench top were displaced (c3).

Dissolution rates of protective coatings

Following the observation of the device degradation and dissolution of SiN_x *in vivo*, we measured the dissolution rate of SiN_x, SiC, and SiO_2 films under accelerated aging test conditions—soaking the devices in saline at 87 °C.

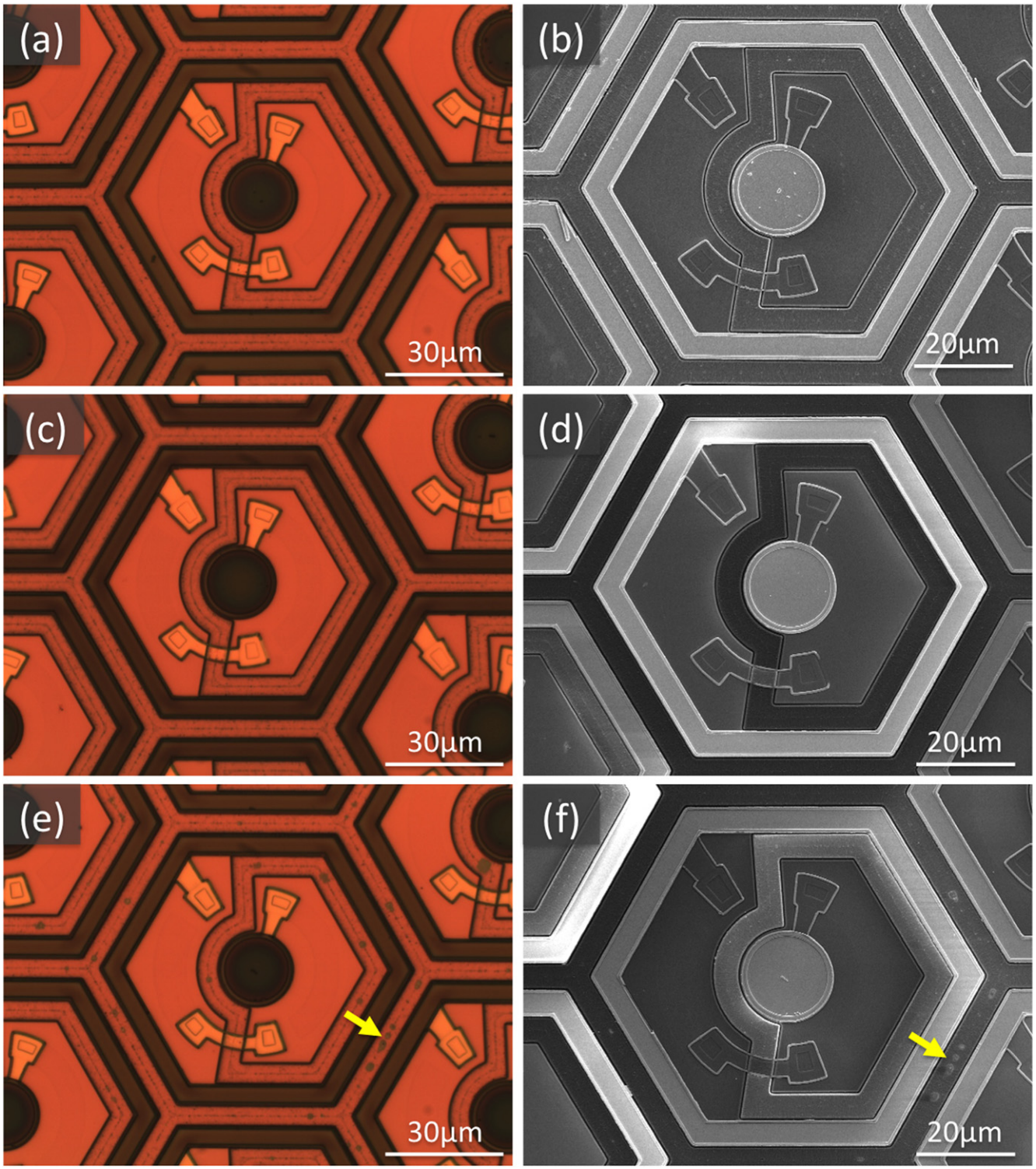

Figure 4. Retinal prostheses (Type I) with 240 nm SiC coating. (a) and (b) A 2-diode pixel before implantation. (c)–(f) Four months after subretinal implantation in a rat eye. (c) and (d) exhibits no signs of degradation, while (e) and (f) showed small patches of color change in the middle of the polysilicon-filled trench (arrows), indicating defects in the SiC film.

SiN_x exhibited a highly reproducible and linear dissolution rate of $18.3 \pm 0.3\,\mathrm{nm\,d^{-1}}$ (single surface) over the course of 28 d at 87 °C (figure 5(a)). In addition, water penetration and bubbling was visible by day 1, and color changes indicative of thinning occurred throughout the course of soaking. By day 28, white dots appeared, suggesting wafer oxidation. Overnight between days 28 and 29, the remaining silicon nitride on each sample (15–23 nm per side) dissolved, and the wafers oxidized extensively. This result corresponded well with the observations *in vivo*, where SiN_x films on the retinal prostheses completely dissolved after 4 months.

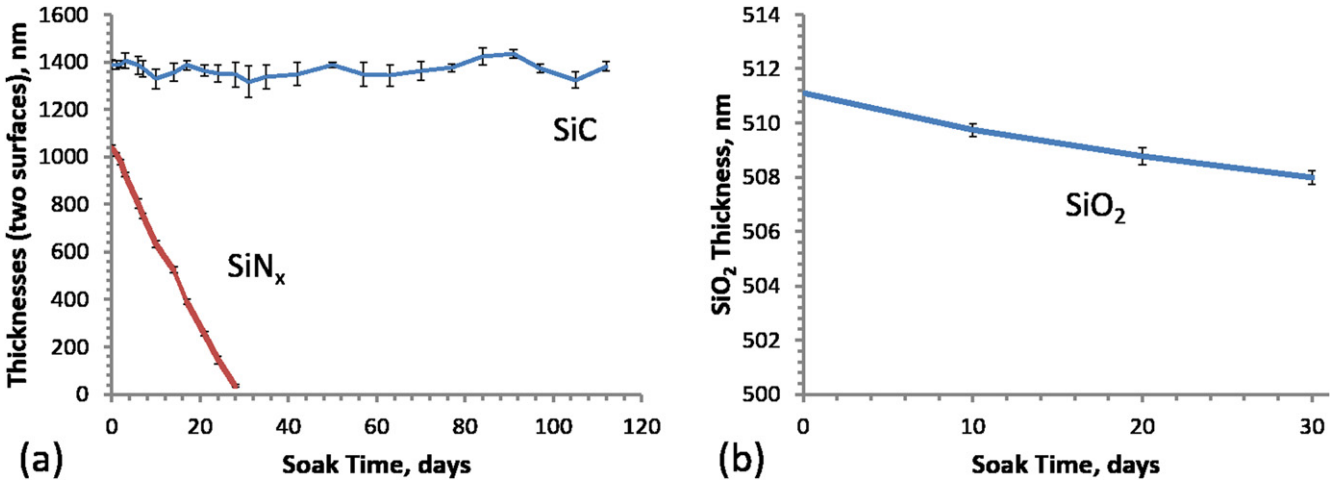

Figure 5. Dissolution rate of dielectric materials in saline at 87 °C. (a) PECVD SiN_x dissolved at 18.3 ± 0.3 nm d^{-1}, while PECVD SiC showed no quantifiable dissolution up to 112 d. (b) Thermal SiO_2 dissolved at 0.104 ± 0.008 nm d^{-1} (data were normalized to the average thickness of SiO_2 on day 0).

In contrast, the five samples coated with SiC exhibited excellent stability. After more than 16 weeks in LPS at 87 °C, they showed neither visible degradation nor quantifiable dissolution (figure 5(a)). This result is in agreement with the earlier measurement of SiC dissolution rate over 28 d at 90 °C [41], and explains why SiC-coated devices were much more stable *in vivo*. The measured film thickness fluctuated within ~2% (standard deviation) over the course of soaking—likely an artifact of the peak fitting procedure. Defects in the SiC films could also contribute to variation in the measurement, if silicon under the defects oxidizes and dissolves, forming localized corrosion that could scatter light during the FTIR measurements.

Thermally grown SiO_2 dissolved very slowly but steadily at 0.104 ± 0.008 nm d^{-1} in saline at 87 °C (figure 5(b)). Thus a SiO_2 coating of 70 nm would last for ~700 d under the accelerated aging conditions, corresponding to tens of years *in vivo*. This explains why the single-crystal silicon part of the implant did not degrade *in vivo* after 1 year, with 70–80 nm of SiO_2 covering it.

Defect analysis

Continuity of the protective coatings is critical for device longevity. Any defect in the film will expose the underlying materials to the harsh environment. Figure 5 demonstrates a measurable dissolution rate of SiN_x and SiO_2, while the thickness of SiC did not change over the course of soaking tests. Therefore, we only performed defect analysis on SiC films deposited on different structures to find weak points in these films, which may lead to degradation of the devices.

For 560 nm SiC films, examination of a total area of 11 cm^2 of the top surface of Type III structures showed no defects (figure 6(a)). Occasional defects were found on the sidewalls of the trenches covered with SiC (figure 6(b)). The scalloping on the sidewall due to the Bosch process likely increased the defect occurrence. SiC covered the trench sidewalls and bottoms continuously to the bottom (figures 7(a) and (b)). For 180 nm SiC films, the trench sidewalls were covered by SiC only down to ~4.5 μm depth (figures 7(c) and (e)). A thin layer (tens of nanometers) of SiC covered the bottom of the trenches. Overhanging SiC films at the corners are visible (figure 7(d)) and are emphasized by deliberately etching the underlying SiO_2 layer.

Similar tests on Type II arrays coated with 240 nm SiC films revealed defects exclusively in the middle of the polysilicon-filled trenches (figure 8(b)). This result matches well the defects observed after the 4 month *in vivo* implantation (figures 4(e) and (f)). For samples coated with 560 nm SiC, no defects were found anywhere on the structures (figure 8(d)). The defect density in SiC films depended on both the device topography and the film thickness. The 5 μm wide trenches were oxidized and filled with polysilicon for electrical isolation and mechanical support (figure 9(a)). The middle of the trenches has a small seam where polysilicon grown from the sidewalls joins (indicated by the arrow in figure 9(b)). The small gaps near the surface are likely to result in defects, if not adequately covered. The 240 nm of SiC coating did not cover these gaps (figure 9(c)), while a 560 nm layer completely coated the gaps (figure 9(d)). Therefore, to properly protect the steps on the surface of the device and eliminate the associated defects in the SiC films, a minimum thickness of the coating, which depends on the topography of the device, must be used. For our retinal prostheses, a SiC thickness of 560 nm appears to provide sufficient protection, although this must still be confirmed pending the 1 year *in vivo* follow-up.

Discussion

Devices not coated with SiC exhibited considerable degradation after 4 months *in vivo*, as shown in figure 2. Devices with open trenches around each pixel (figure 2(c)) exhibited more erosion than the ones with filled trenches (figure 2(b)). But regardless the extent of degradation, the fact that it is noticeable in all uncoated devices indicates the need for a good protective coating.

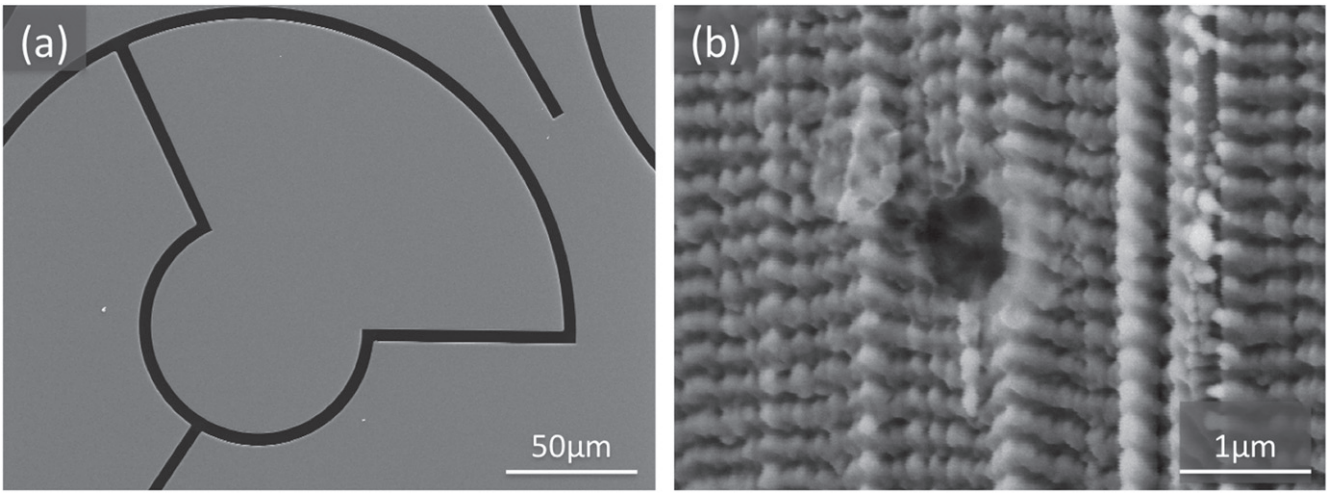

Figure 6. Defect characterization of SiC films (Type III). (a) Top view of 560 nm SiC film deposited on a smooth surface of 480 nm thermal SiO_2 on a bulk Si substrate with etched and oxidized trenches. No defects were found on 11 cm^2 of the top surface examined. (b) A defect on a trench sidewall.

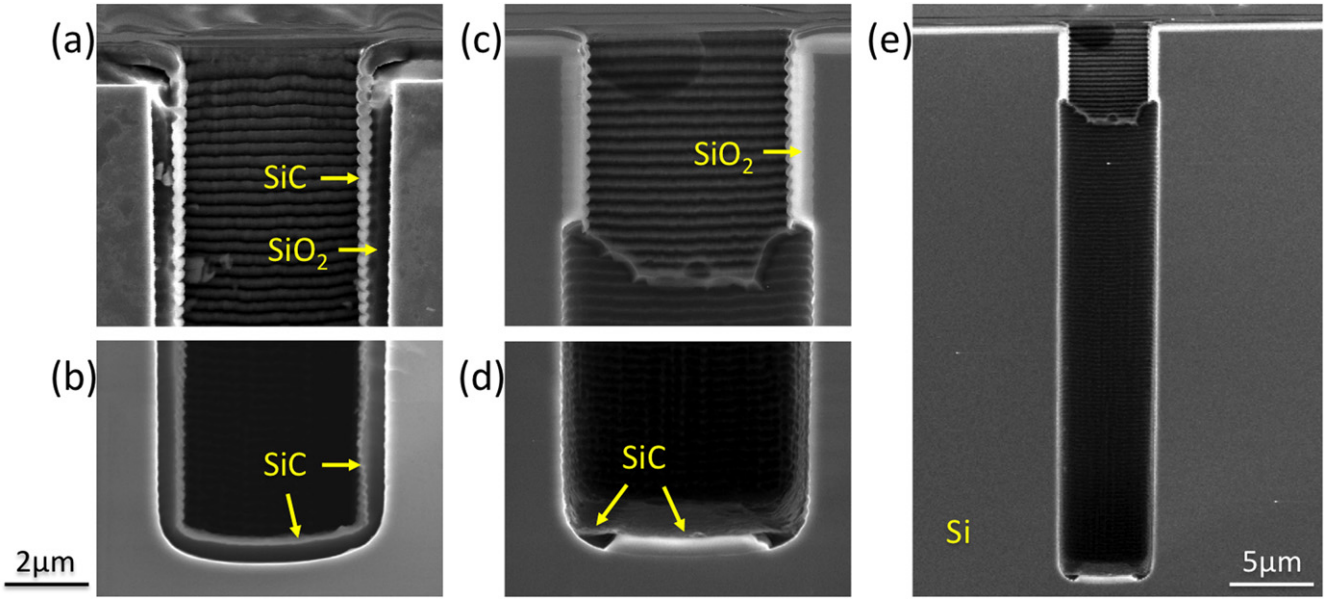

Figure 7. Trench coverage of SiC films (Type III). (a) and (b) 560 nm SiC deposited on 480 nm SiO_2 on a bulk Si substrate with etched and oxidized trenches. The continuous SiC film on the sidewall and bottom is pointed out by the arrows. (c)–(e) 180 nm SiC deposited on 480 nm SiO_2 on Si substrate with etched and oxidized trenches. The SiC film was continuous only at the top ~4.5 μm of the trench.

SiC films appear to protect the silicon wafers very well: we have not observed dissolution of this coating in accelerated aging, nor any defects in thick (~1 μm) SiC films deposited on flat surfaces. However, we observed a few defects or weak spots in 200–300 nm thick SiC films in the middle of the filled trenches (figure 8(b)), where the surface of the underlying polysilicon is not smooth (figure 9(c)). Eliminating such seams in the trenches would improve the stability of such devices. Alternatively, using thicker SiC can completely cover these rough features, as shown in figure 9(d) with 560 nm coating.

Si(001) is known to dissolve in saline along preferential crystallographic planes, generating rectangular or square defects [43]. Silicon also reacts actively with many biological enzymes and fluids [49, 50] and degrades after interactions with cell cultures [51]. In aqueous media, SiN_x is oxidized to form SiO_2 and NH_3, and SiO_2 hydrolyzes into $Si(OH)_4$ [52–54]. Therefore, a silicon implant with SiO_2 and SiN_x coatings will not survive long enough for chronic human use. SiC is known to react with O_2 and H_2O at very high temperatures (800 °C–1000 °C) [55–57], however, it is chemically inert under physiological conditions. Except for a possible observation of SiC surface oxidation [43], no chemical reactions involving SiC under physiological conditions have been reported.

To estimate the SiC coating lifetime, we assumed an acceleration factor of $2^{\Delta T/10}$, which has been used for polymers in medical devices and other applications [58], assuming first-order rate kinetics for the dissolution process. Under this

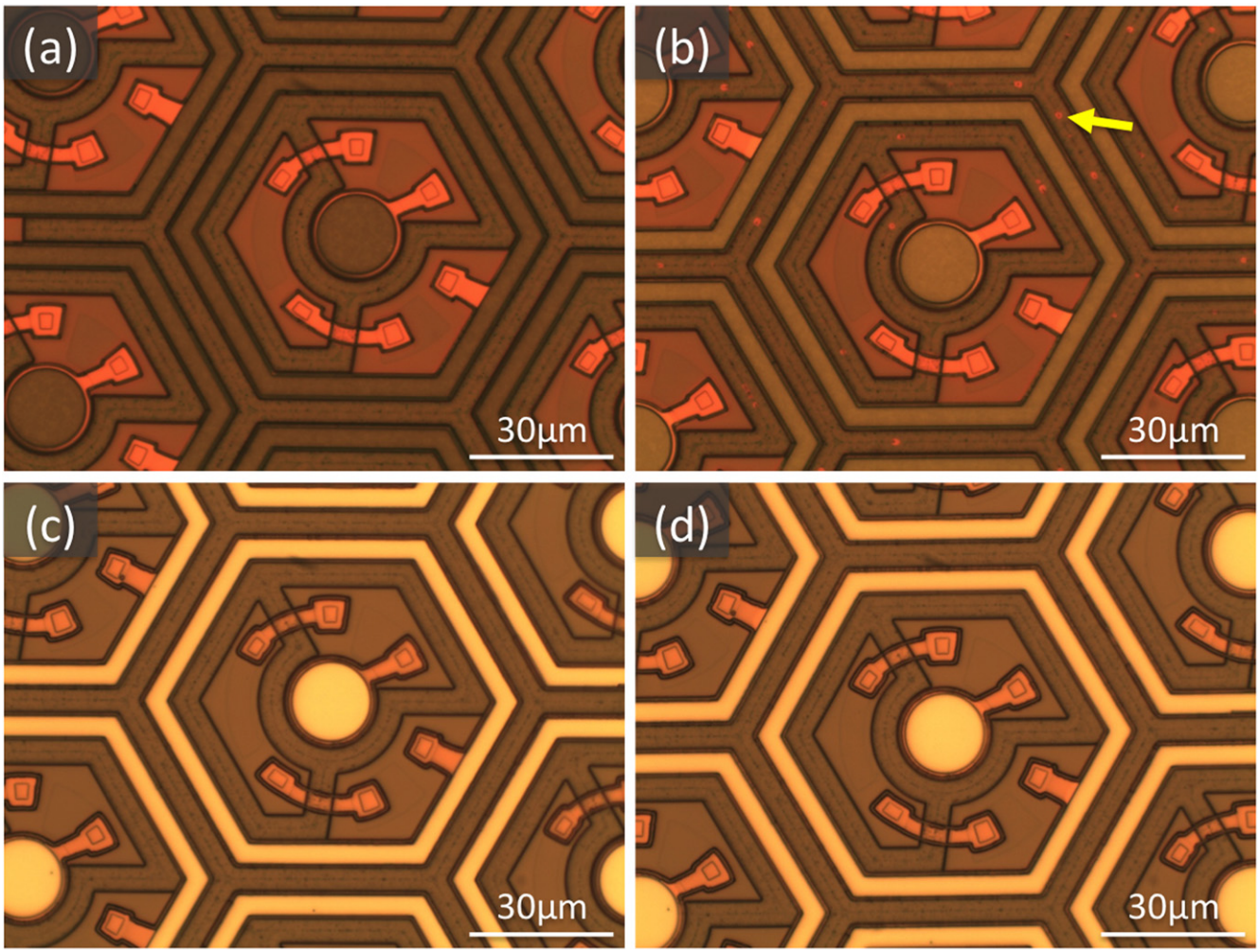

Figure 8. Defect characterization of SiC films deposited on retinal prostheses (Type II). (a) and (b) 3-diode array with 240 nm of SiC. (c) and (d) 3-diode array with 560 nm of SiC. (b) and (d) After etching in BOE 6:1 for 10 min to reveal defects in the SiC films. (b) With 240 nm SiC, defects were visible in the middle of polysilicon filled trenches (arrow). (d) No defects were visible with 560 nm SiC.

scheme, the aging factor at 87 °C compared to physiological temperature (37 °C) is $2^{(87\text{-}37)/10} = 2^5 = 32$, which means that a day of accelerated aging corresponds to about a month at physiological temperature. In this study, the SiC coatings did not change after 112 d at 87 °C, translating to no detectable degradation for roughly 10 years under physiological conditions.

Dissolution of SiN_x coatings and polysilicon in the trenches was the primary cause of device failure in this study. Eliminating SiN_x and polysilicon should greatly increase the lifetime of the devices. SiC can not only replace SiN_x as the protective coating, but also serve as a part of the anti-reflective coating for the retinal implant, in combination with the underlying SiO_2. Simulation by the transfer matrix method [59, 60] (figure 10) showed that 560 nm of SiC on top of 310–380 nm of SiO_2 could reduce reflection of 880 nm light below 10% at vertical incidence. SiO_2 and SiC films of such thickness exhibit low defect densities even in areas of complex topography, and therefore can provide effective protection.

The backside of the retinal prostheses can be coated with SiC at a much lower temperature to be compatible with the sputtered iridium oxide film (SIROF) electrode used in our devices. Amorphous SiC can be deposited at 175 °C by electron cyclotron resonance PECVD [61], at <200 °C by PECVD [43, 62], and even at room temperature by RF magnetron sputtering [63], although the stability of those films in saline solution needs to be investigated. Therefore, SiC coating can be deposited after SIROF deposition and release of the devices. Sidewalls of the devices can be coated with SiC by a combination of depositions from the top and bottom. Alternatively, the back and sidewalls of the implant can be coated with metal.

Aside from increasing the SiC film thickness, the defect density can be reduced by growth interruption during the SiC deposition. The defects in SiC films on the trench sidewalls can also be reduced by decreasing the scalloping related to the Bosch process used to etch trenches in the silicon. H_2 annealing at an elevated temperature has been demonstrated to smooth sidewalls [64–66].

The dissolution rate of SiC and other dielectric materials might be different with an electric field applied. Further study of the retinal prostheses *in vivo* with chronic photovoltaic activation will shed more light on this topic.

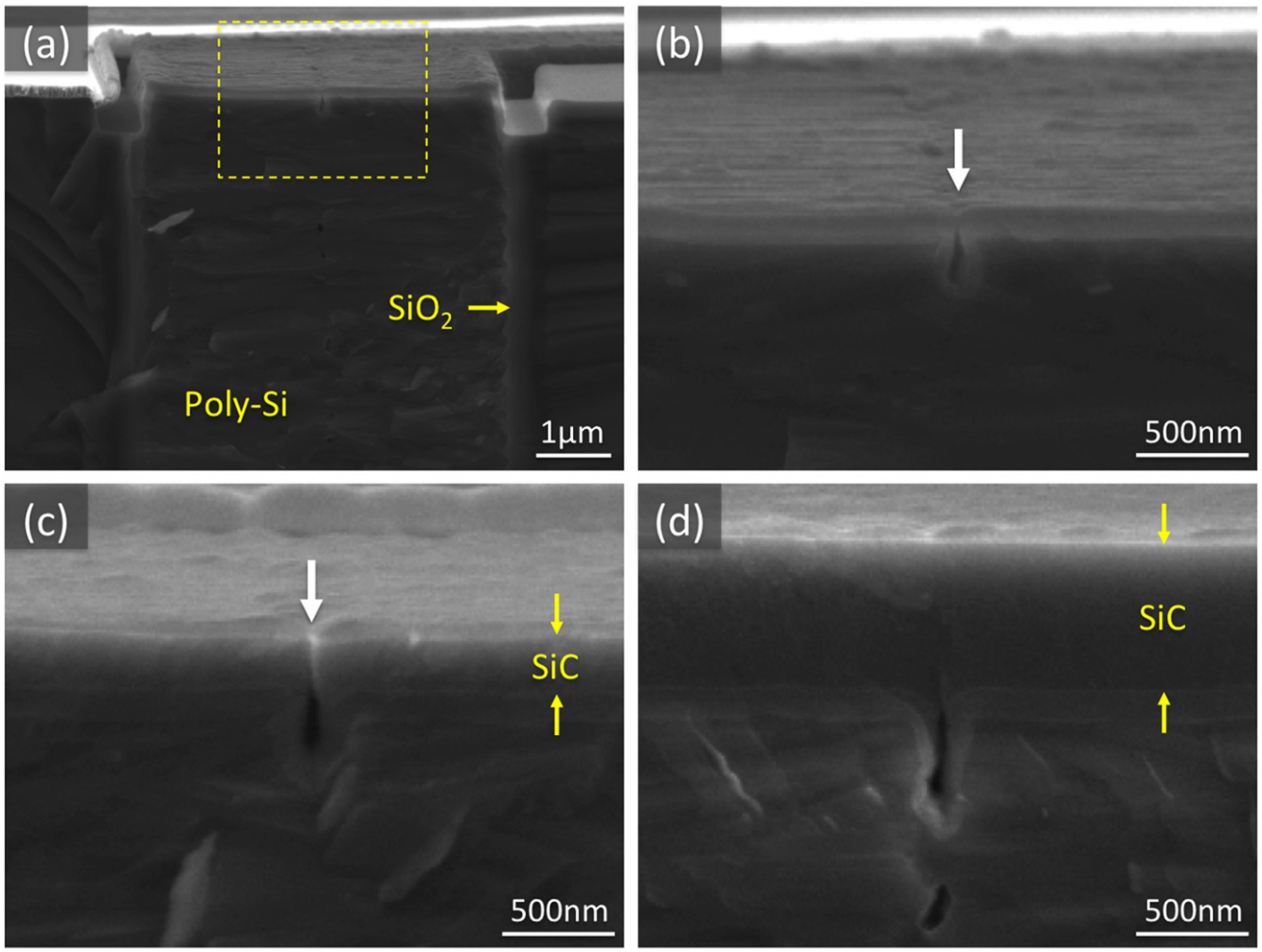

Figure 9. Cross-section of retinal prostheses (Type II) in the trench region. (a) Sample with no SiC coating, showing the top ~5 μm of the polysilicon-filled trench. (b) Zoom-in image of the middle of the trench (yellow dashed rectangle) of (a). White arrow points to the gap in polysilicon. (c) A sample with 240 nm SiC coating. Small gap in the middle of the trench not fully covered by SiC is indicated by the white arrow. (d) Sample with 560 nm SiC coating completely covering the gap.

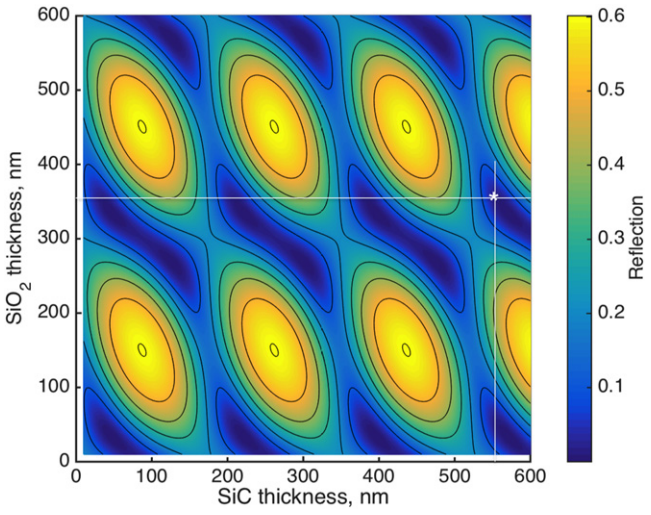

Figure 10. Calculated optical reflectivity of the SiC and thermal SiO_2 stack in saline. 560 nm of SiC on top of 310–380 nm of SiO_2 could reduce reflection of 880 nm light below 10% at vertical incidence.

Conclusions

Significant degradation of unprotected photovoltaic retinal prostheses was found after 4 month implantation, especially in the polysilicon-filled trenches. PECVD SiC films were much more effective than SiN_x and SiO_2 coatings in protecting the devices *in vivo*. Accelerated aging tests did not change the thickness of SiC film after 112 d in saline at 87 °C. The SiN_x coating was much less stable, and dissolved at $18.3 \pm 0.3\,\text{nm}\,\text{d}^{-1}$ at 87 °C. Thermal SiO_2 grown at high temperature (1000 °C) was more stable, but still dissolved very slowly at $0.104 \pm 0.008\,\text{nm}\,\text{d}^{-1}$ at 87 °C in saline. SiC films exhibited some defects on complicated topography and rough surfaces. The defect density could be reduced or eliminated by smoothening the underlying surface or by increasing the SiC film thickness. Overall, PECVD SiC films have desirable properties as protective coatings for implantable electronics. A combination of thermal SiO_2 with a PECVD SiC film should be adequate for providing anti-reflective coating and protecting retinal prostheses for long-term use.

Acknowledgments

Funding was provided by the US National Institutes of Health (grant R01-EY-018608, D P), the Department of Defense (grant W81XWH-15-1-0009, D P), and the Stanford Spectrum fund (D P). K M was supported by an SU2P fellowship as part of a RCUK Science Bridges award. H L was supported in part by the Foundation Voir et Entendre (Paris) and Pixium Vision. Fabrication was performed in part at the Stanford Nanofabrication Facility, which is supported by National Science Foundation through the NNIN (grant ECS-9731293). Sample preparation by SEM (FEI XL30 Sirion) was performed at the Stanford Nano Shared Facilities (SNSF). Accelerated SiC degradation testing at EIC Laboratories was performed partly by Doug Orsi and Chathuri Gunasekharan.

References

[1] Crosby P A, Daly C N, Money D K, Patrick J F, Seligman P M and Kuzma J A 1985 Cochlear implant system for an auditory prosthesis *US Patent Specification* 4,532,930

[2] McDermott H 1989 An advanced multiple channel cochlear implant *IEEE Trans. Biomed. Eng.* **36** 789–97

[3] Wilson B S, Finley C C, Lawson D T, Wolford R D, Eddington D K and Rabinowitz W M 1991 Better speech recognition with cochlear implants *Nature* **352** 236–8

[4] Benabid A L, Pollak P, Gao D, Hoffmann D, Limousin P, Gay E, Payen I and Benazzouz A 1996 Chronic electrical stimulation of the ventralis intermedius nucleus of the thalamus as a treatment of movement disorders *J. Neurosurg.* **84** 203–14

[5] Limousin P, Krack P, Pollak P, Benazzouz A, Ardouin C, Hoffmann D and Benabid A L 1998 Electrical stimulation of the subthalamic nucleus in advanced Parkinson's disease *N. Engl. J. Med.* **339** 1105–11

[6] Kumar R, Lozano A M, Kim Y J, Hutchison W D, Sime E, Halket E and Lang A E 1998 Double-blind evaluation of subthalamic nucleus deep brain stimulation in advanced Parkinson's disease *Neurology* **51** 850–5

[7] Kupsch A *et al* 2006 Pallidal deep-brain stimulation in primary generalized or segmental dystonia *N. Engl. J. Med.* **355** 1978–90

[8] Hochberg L R, Serruya M D, Friehs G M, Mukand J A, Saleh M, Caplan A H, Branner A, Chen D, Penn R D and Donoghue J P 2006 Neuronal ensemble control of prosthetic devices by a human with tetraplegia *Nature* **442** 164–71

[9] Hochberg L R *et al* 2012 Reach and grasp by people with tetraplegia using a neurally controlled robotic arm *Nature* **485** 372–5

[10] Shenoy K V, Sahani M and Churchland M M 2013 Cortical control of arm movements: a dynamical systems perspective *Annu. Rev. Neurosci.* **36** 337–59

[11] Campbell P K, Jones K E, Huber R J, Horch K W and Normann R A 1991 A silicon-based, three-dimensional neural interface: manufacturing processes for an intracortical electrode array *IEEE Trans. Biomed. Eng.* **38** 758–68

[12] Normann R A, Maynard E M, Rousche P J and Warren D J 1999 A neural interface for a cortical vision prosthesis *Vis. Res.* **39** 2577–87

[13] Zrenner E *et al* 2011 Subretinal electronic chips allow blind patients to read letters and combine them to words *Proc. Biol. Sci.* **278** 1489–97

[14] Ahuja A K, Dorn J D, Caspi A, McMahon M J, Dagnelie G, Dacruz L, Stanga P, Humayun M S, Greenberg R J and Argus II Study Group 2011 Blind subjects implanted with the Argus II retinal prosthesis are able to improve performance in a spatial-motor task *Br. J. Ophthalmol.* **95** 539–43

[15] Humayun M S *et al* 2012 Interim results from the international trial of second sight's visual prosthesis *Ophthalmology* **119** 779–88

[16] Mathieson K *et al* 2012 Photovoltaic retinal prosthesis with high pixel density *Nat. Photon.* **6** 391–7

[17] Lorach H *et al* 2015 Photovoltaic restoration of sight with high visual acuity *Nat. Med.* **21** 476–82

[18] Jensen R J and Rizzo J F III 2006 Thresholds for activation of rabbit retinal ganglion cells with a subretinal electrode *Exp. Eye Res.* **83** 367–73

[19] Anderson D J, Najafi K, Tanghe S J, Evans D A, Levy K L, Hetke J F, Xue X L, Zappia J J and Wise K D 1989 Batch-fabricated thin-film electrodes for stimulation of the central auditory system *IEEE Trans. Biomed. Eng.* **36** 693–704

[20] Hetke J F, Lund J L, Najafi K, Wise K D and Anderson D J 1994 Silicon ribbon cables for chronically implantable microelectrodes arrays *IEEE Trans. Biomed. Eng.* **41** 314–21

[21] Weiland J D and Anderson D J 2000 Chronic neural stimulation with thin-film, iridium oxide electrodes *IEEE Trans. Biomed. Eng.* **47** 911–8

[22] Plummer J D, Deal M D and Griffin P B 2000 *Silicon VLSI Technology* (Upper Saddle River, NJ: Prentice-Hall) p 725

[23] Hämmerle H, Kobuch K, Kohler K, Nisch W, Sachs H and Stelzle M 2002 Biostability of micro-photodiode arrays for subretinal implantation *Biomaterials* **23** 797–804

[24] Loeb G E, Bak M J, Salcman M and Schmidt E M 1977 Parylene as a chronically stable, reproducible microelectrode insulator *IEEE Trans. Biomed. Eng.* **24** 121–8

[25] Hsu J M, Rieth L, Normann R A, Tathireddy P and Solzbacher F 2009 Encapsulation of an integrated neural interface device with Parylene C *IEEE Trans. Biomed. Eng.* **56** 23–9

[26] Xie X, Rieth L, Williams L, Negi S, Bhandari R, Caldwell R, Sharma R, Tathireddy P and Solzbacher F 2014 Long-term reliability of Al_2O_3 and Parylene C bilayer encapsulated Utah electrode array based neural interfaces for chronic implantation *J. Neural Eng.* **11** 1–9

[27] Charmet J, Bitterli J, Sereda O, Liley M, Renaud P and Keppner H 2013 Optimizing Parylene C adhesion for MEMS processes: potassium hydroxide wet etching *J. Microelectromech. Syst.* **22** 855–64

[28] Chen T N, Wuu D S, Wu C C, Chiang C C, Chen Y P and Horng R H 2006 High-performance transparent barrier films of SiO_x/SiN_x stacks on flexible polymer substrates *J. Electrochem. Soc.* **153** F244–8

[29] Potts S E *et al* 2011 Ultra-thin aluminium oxide films deposited by plasma-enhanced atomic layer deposition for corrosion protection *J. Electrochem. Soc.* **158** 132–8

[30] Roy R K and Lee K R 2007 Biomedical applications of diamond-like carbon coatings: a review *J. Biomed. Mater. Res. B Appl. Biomater.* **83** 72–84

[31] Xiao X, Birrell J, Gerbi J E, Auciello O and Carlisle J A 2004 Low temperature growth of ultrananocrystalline diamond *J. Appl. Phys.* **96** 2232–9

[32] Xiao X *et al* 2006 In vitro and in vivo evaluation of ultrananocrystalline diamond for coating of implantable retinal microchips *J. Biomed. Mater. Res. B Appl. Biomater.* **77** 273–81

[33] Chen Y C, Tsai C Y, Lee C Y and Lin I N 2014 In vitro and in vivo evaluation of ultrananocrystalline diamond as an encapsulation layer for implantable microchips *Acta Biomater.* **10** 2187–99

[34] Bolz A, Amon M, Ozbek C, Heublein B and Schaldach M 1996 Coating of cardiovascular stents with a semiconductor to improve their hemocompatibility *Tex. Heart Inst. J.* **23** 162–6
[35] Amon M, Bolz A and Schaldach M 1996 Improvement of stenting therapy with a silicon carbide coated tantalum stent *J. Mater. Sci.—Mater. Med.* **7** 273–8
[36] Rzany A and Schaldach M 2001 Smart material silicon carbide: reduced activation of cells and proteins on a SiC:H-coated stainless steel *Prog. Biomed. Res.* **6** 182–94
[37] Chang C Y, Fang Y K, Huang C F and Wu B S 1985 Novel passivation dielectrics—the boron- or phosphorus-doped hydrogenated amorphous silicon carbide films *J. Electrochem. Soc.* **132** 418–22
[38] Loboda M J and Michael K W 1998 Silicon carbide metal diffusion barrier layer *United States Patent* 5,818,071
[39] Merchant S M, Misra S and Roy P K 2000 Silicon carbide barrier layers for porous low dielectric constant materials *US Patent Specification* 6,100,587
[40] Nemani S, Xia L Q and Yieh E 2002 Dual frequency plasma enhanced chemical vapor deposition of silicon carbide layers *US Patent Specification* 6,465,366 B1
[41] Cogan S F, Edell D J, Guzelian A A, Liu Y P and Edell R 2003 Plasma-enhanced chemical vapor deposited silicon carbide as an implantable dielectric coating *J. Biomed. Mater. Res.* A **67** 856–67
[42] Maloney J M, Lipka S A and Baldwin S P 2005 In vivo biostability of CVD silicon oxide and silicon nitride films *Mater. Res. Soc. Symp. Proc.* **872** J14.3
[43] Hsu J M, Tathireddy P, Rieth L, Normann A R and Solzbachera F 2007 Characterization of a-SiC$_x$:H thin films as an encapsulation material for integrated silicon based neural interface devices *Thin Solid Films* **516** 34–41
[44] Bai Q, Wise K D and Anderson D J 2000 A high-yield microassembly structure for three-dimensional microelectrode arrays *IEEE Trans. Biomed. Eng.* **47** 281–9
[45] Wang L *et al* 2012 Photovoltaic retinal prosthesis: implant fabrication and performance *J. Neural Eng.* **9** 1–11
[46] Boinagrov D, Pangratz-Fuehrer S, Goetz G and Palanker D 2014 Selectivity of direct and network-mediated stimulation of the retinal ganglion cells with epi-, sub- and intraretinal electrodes *J. Neural Eng.* **11** 026008
[47] Mandel Y *et al* 2013 Cortical responses elicited by photovoltaic subretinal prostheses exhibit similarities to visually evoked potentials *Nat. Commun.* **4** 1–9
[48] Ahn S, Spuhler P S, Chiari M, Cabodi M and Ünlü M S 2012 Quantification of surface etching by common buffers and implications on the accuracy of label-free biological assays *Biosens. Bioelectron.* **36** 222–9
[49] Birchall J D and Chappell J S 1988 The chemistry of aluminum and silicon in relation to Alzheimer's disease *Clin. Chem.* **34** 265–7
[50] Bayliss S C, Buckberry L D, Harris P J and Tobin M 2000 Nature of the silicon–animal cell interface *J. Porous Mater.* **7** 191–5
[51] Saddow S E 2012 *Silicon Carbide Biotechnology* (Amsterdam: Elsevier)
[52] Osenbach J W and Knolle W R 1992 Behavior of a-SiN:H and a-SiON:H films in condensed water *J. Electrochem. Soc.* **139** 3346–51
[53] Vogt M and Hauptmann R 1995 Plasma-deposited passivation layers for moisture and water protection *Surf. Coat. Technol.* **74–75** 676–81
[54] Schmitt G, Schultze J W, Faßbender F, Buß G, Lüth H and Schöning M J 1999 Passivation and corrosion of microelectrode arrays *Electrochim. Acta* **44** 3865–83
[55] Munro R G and Dapkunas S J 1993 Corrosion characteristics of silicon carbide and silicon nitride *J. Res. Natl Inst. Stand. Technol.* **98** 607–31
[56] Kraft T, Nickel K G and Gogotsi Y G 1998 Hydrothermal degradation of chemical vapour deposited SiC fibres *J. Mater. Sci.* **33** 4357–64
[57] Pastila P, Helanti V, Nikkilä A and Mäntylä T 2001 Environmental effects on microstructure and strength of SiC-based hot gas filters *J. Eur. Ceram. Soc.* **21** 1261–8
[58] Hukins D W, Mahomed A and Kukureka S N 2008 Accelerated aging for testing polymeric biomaterials and medical devices *Med. Eng. Phys.* **30** 1270–4
[59] Knittl Z 1976 *Optics of Thin Films* (London: Wiley)
[60] Pettersson L A, Roman L and Sand Inganäs O 1999 Modeling photocurrent action spectra of photovoltaic devices based on organic thin films *J. Appl. Phys.* **86** 487–96
[61] Loboda M J 1992 Low temperature PECVD growth and characterization of a-SiC:H films deposited from silacyclobutane and silane/methane precursor gases *Springer Proc. Phys.* **71** 271–80
[62] Jiang L, Chen X, Wang X, Xu L, Stubhan F and Merkel K 1999 a-SiC$_x$-H films deposited by plasma-enhanced chemical vapor deposition at low temperature used for moisture and corrosion resistant applications *Thin Solid Films* **352** 97–101
[63] Ledermann N, Baborowski J, Muralt P, Xantopoulos N and Tellenbach J M 2000 Sputtered silicon carbide thin films as protective coating for MEMS applications *Surf. Coat. Technol.* **125** 246–50
[64] Sato T, Mitsutake K, Mizushima I and Tsunashima Y 2000 Micro-structure transformation of silicon: a newly developed transformation technology for patterning silicon surfaces using the surface migration of silicon atoms by hydrogen annealing *Japan. J. Appl. Phys.* **39** 5033–8
[65] Kuribayashi H, Hiruta R, Shimizu R, Sudoh K and Iwasaki H 2003 Shape transformation of silicon trenches during hydrogen annealing *J. Vac. Sci. Technol.* A **21** 1279–83
[66] Lee M C M and Wu M C 2006 Thermal annealing in hydrogen for 3D profile transformation on silicon-on-insulator and sidewall roughness reduction *J. Microelectromech. Syst.* **15** 338–43